

# A machine learning approach for efficient and robust resistance spot welding monitoring

Lars Bogaerts<sup>1\*</sup>, Arnout Dejans<sup>1</sup>, Matthias Faes<sup>2</sup> and David Moens<sup>1</sup>

<sup>1\*</sup>Department of Mechanical Engineering – LMSD division, KU Leuven, Jan De Nayerlaan 5, St.-Katelijne-Waver, 2860, Belgium.

<sup>2</sup>Chair for Reliability Engineering, TU Dortmund University, Leonhard-Euler-Strasse 5, Dortmund, 44227, Germany.

\*Corresponding author(s). E-mail(s): [lars.bogaerts\[at\]kuleuven.be](mailto:lars.bogaerts@kuleuven.be);

Contributing authors: [Arnout.dejans\[at\]kuleuven.be](mailto:Arnout.dejans@kuleuven.be); [matthias.faes\[at\]tu-dortmund.de](mailto:matthias.faes@tu-dortmund.de); [david.moens\[at\]kuleuven.be](mailto:david.moens@kuleuven.be);

## Abstract

The estimation of the weld nugget diameter generated by the resistance spot welding process is a crucial element in the assessment of the overall quality of the weld and plays a major role in in-line process control. The process is crucial to produce end-products in many industries such as aviation, aerospace, automotive and other industrial areas. A modern car body contains typically several thousands of welds produced by resistance spot welding, setting an ideal scene for in-line process control. Current state of the art monitoring methods are based on several features extracted from the dynamic resistance signal. However, the accuracy of those is generally not high. In this work, a method for predicting the nugget diameter based on the combination of unsupervised deep learning and Gaussian process regression is developed. Autoencoders are adopted to extract features from the dynamic resistance curve in a low dimensional representation. These features embody underlying information on the process, possibly unobservable or not detectable by any other currently existing approach. Next, a Gaussian process regression model is trained to link those features to the target weld nugget diameter. Compared with the currently popular geometrical attributes approach, the results show that the model has a higher prediction accuracy in nugget diameter prediction, whilst remaining a low cost implementation in an industrial setting. These results are supported by several cases, derived directly from common industrial bottlenecks. Both cases indicate a strong potential with the new AE-GPR approach, with consistently improved results compared to the currently popular geometrical attributes approach.

**Keywords:** Resistance spot welding, Nugget diameter, deep learning, machine learning

## 1 Introduction

Resistance spot welding (RSW) is a highly efficient, low cost and easy realisable joining technique. The technique has been used extensively and is crucial to produce end-products in many

industries such as aviation, aerospace, automotive and other industrial areas. The process employs two welding electrodes that press two or more overlapping sheet-like workpieces together. The heat generated by the then-applied electric current, in correspondence with Joule's law, causes

12 local melting at the workpiece's common faying 63  
13 surface, leading to joining these workpieces. This 64  
14 ease of operation contributed vastly to the quality 65  
15 and automation of the production of modern car 66  
16 bodies, which contain typically several thousands 67  
17 of welds produced by RSW. The safety and reli- 68  
18 ability of current automobile industry is only one 69  
19 of many examples that notably profited from the 70  
20 valuable RSW process.

21 To a large extent, this success can be 72  
22 attributed to the ease of automation of the RSW 73  
23 process in an assembly line. Further, RSW also 74  
24 combines high strength joining with production 75  
25 flexibility, low cost and fast throughput. Thanks 76  
26 to its wide-spread use, RSW has grown to a 77  
27 mature joining technique, with literature dating 78  
28 back to the second half of the 19th century (exper- 79  
29 imentally oriented) [8] and early 2000's (on-line 80  
30 monitoring, Finite Element methods) [12, 13]. 81  
31 Yet, in industrial practice, it still suffers from a 82  
32 high sensitivity to often uncontrollable and vari- 83  
33 able process conditions. This makes the RSW 84  
34 process extremely vulnerable to environmental 85  
35 effects, surface conditions, misalignment, wear, 86  
36 etc. Inevitably, abnormal welding conditions dra- 87  
37 matically reduce the consistency of welds, which 88  
38 generally leads to significant degradation of the 89  
39 weld quality. Therefore, it is a vital task to con- 90  
40 trol and monitor the quality of the welding process 91  
41 [10]. Also, in order to increase productivity and 92  
42 achieve a robust final assembly, an attempt to 93  
43 minimise the number of required spot welds is 94  
44 made. This is only possible when consistent and 95  
45 sufficient weld quality can be guaranteed [23, 32]. 96  
46 For the latter, a common technique remains non- 97  
47 destructive testing, based on a random subset of 98  
48 the workpieces on the production site. However, 99  
49 these weld quality estimations can only be exam- 100  
50 ined off-line, making it impossible to receive brisk 101  
51 and pertinent information. Furthermore, it is very 102  
52 cost inefficient for mass production environments, 103  
53 where RSW is vastly present.

54 In the context of process monitoring, real-time 105  
55 weld quality estimation based on data-driven tech- 106  
56 niques are becoming ever more common [3, 11, 21]. 107  
57 These approaches typically link process param- 108  
58 eters and on-line measurements to product quality 109  
59 metrics in order to guard the process. In this 110  
60 respect, machine learning approaches yield very 111  
61 fast black-box models enabling on-line application 112  
62 for process control. However, multiple problems

arise with these black-box models: (a) These mod-  
els are known to have only limited value when  
extrapolation is required. Their use is most rel-  
evant for well-confined and -controlled processes  
that enable the generation of a clear, industri-  
ally representative and comprehensive data set for  
the model training. There are large discrepancies  
between a lab-environment or numerically-made  
data-set and an industrial data-set, which is prone  
to inaccuracy due to changing variables or bound-  
ary conditions that come with the large change in  
environment. (b) Quantitative measurement capa-  
bilities for the process response are limited in  
the RSW process, hence eliminating the indus-  
trial applicability of data-hungry algorithms such  
as most supervised deep-learning toolboxes [20].

Various in-line measurement techniques for the  
RSW process are investigated in literature, and  
can be classified based on the quantity of mea-  
surement (e.g., force, current, time) and their  
corresponding measurement device. Some of these  
techniques show promising results regarding in-  
line prediction of the weld nugget diameter, which  
is usually the primary choice for the Quality Indi-  
cator (QI) of the process [4]. A first class of  
prediction models makes use of mechanical mea-  
surements, e.g., displacements [24], forces [31] or  
acoustic emission [7]. While these are possible  
sources of valuable process information, and state  
of the art technology for measurement of the  
required quantities is proven achievable on indus-  
trial scale, the reliability, accuracy and flexibility  
of these models remain a challenge [25], lead-  
ing to their limited use in an industrial context.  
A second class of techniques focuses on moni-  
toring through electrical signals. In this context,  
dynamic resistance (DR) measurements are widely  
investigated and implemented in industrial prac-  
tice [9, 22, 29]. There are several milestones in  
the progress of monitoring the dynamic resistance.  
In 2002, Cho and Rhee [5] calculated dynamic  
resistance based on current and voltage from the  
primary part of the transformer. Further break-  
throughs include quality estimators by means of  
a Hopfield network, presented in [6], Artificial  
Neural Networks (ANN) [17], welding quality clas-  
sifiers by means of Probabilistic Neural Networks  
(PNN) [27] and a random forest model based on  
features of the dynamic resistance curves [25].  
Measurement of dynamic resistance has become

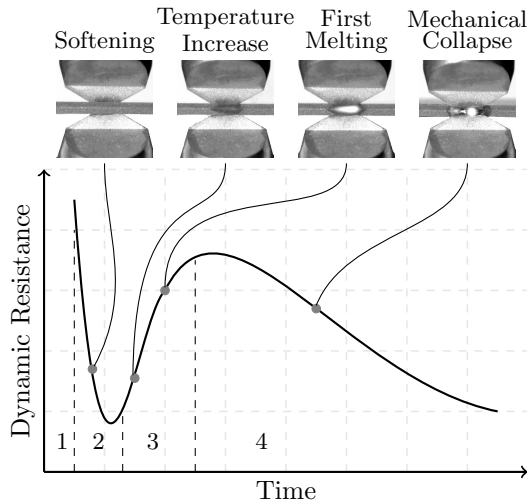


**Fig. 1:** Theoretical dynamic resistance curve interpretation and characterisation. Top images illustrate the evolution of the weld nugget at the given phase and are made by a phantom VEO 640 ultra high speed camera. Based on the original graph of D.W. Dickinson et al. [8]

the accepted paradigm in industry [1, 15, 30], and has been implemented in several commercially available power sources as a quality monitoring and evaluation tool. For this reason, it is selected as primary feature in this work. Furthermore, there is a clear link between the evolution of the weld nugget and the dynamic resistance, as illustrated in figure 1. For more detail on the subject, the reader is referred to [8].

## 1.1 Motivation

While extensive literature exists regarding the online monitoring and the quality assessment of the spot welding process based on dynamic resistance and alternative measurements, many challenges remain. Many of the aforementioned techniques suffer from drawbacks that hinder their optimal cost-effective and fully automated application for RSW processes in industrial practice. These shortcomings are the following.

1. Current dynamic resistance based techniques fail to establish an accurate prediction when variations on the input signal are present, either due to process parameter alterations or inherent randomness in the process.

2. The dynamic resistance curve is containing information that is not necessarily observable in a time signal, and therefore lost by currently existing techniques. Consequently, the widely investigated techniques based on the geometric attributes of the dynamic resistance measurement (see section 3.2) are not fully exploiting their potential.
3. Alternatives for the measurement of dynamic resistance are lacking robustness, mainly due to the type of measurement. This leads to either economical or infrastructural burdens, which render them less interesting for industrial application.

In an effort to remedy these shortcomings, this paper investigates a weld quality monitoring approach based on the underlying parametric dependencies of the dynamic resistance during the RSW process. The weld nugget diameter serves as the main driving Quality Indicator (QI) for this research. The capability of predicting the weld nugget diameter by means of limited measurements is an important aspect of the developed approach. This is important to keep the number of man-hours required to measure the data-set feasible. Furthermore, the technique should be able to cope with variations, re-calibrations or other possible variability within industrial application.

We propose deep learning autoencoders to discover a low dimensional representation that captures the underlying causes of the resistance in the secondary circuit of the welding machine during the RSW process. This allows for a sparse representation that can be leveraged towards in-line prediction of the weld nugget diameter. The method is demonstrated on an experimental dataset to clarify the technique and to compare it with the geometrical attributes approach (elaborated in section 3), by means of computational performance, prediction accuracy, advantages and disadvantages.

Next, the method is demonstrated on several example problems, showing that the technique has large potential on diverse problems.

The paper is structured as follows:

- Section 2 elaborates on the conducted experiments, as well as the required hardware both for experiments, measurements and processing the data,

- Section 3 discusses the geometrical attributes approach, which serves as a reference for the novel methods developed in the next sections,
- Section 4 introduces the autoencoder based approach,
- Section 5 applies the introduced method to two case studies to illustrate its application and performance,
- Section 6 lists the most important conclusions of this manuscript.

## 2 Experimental setup

Experiments described in this work are performed on an ARO servo-driven RSW machine with a 1000 Hz, 90 kVA DC power source, as depicted in figure 2. The machine is equipped with water cooled electrode caps with an ISO 5821:2009 FE-15.8-5.5-30 geometry. Three experiments were conducted using process parameters as summarised in table 1. For each experiment, the complete set of process parameters and the number of realisations  $n$  is provided. Experimental set 1 represents a limited run in a production setup under ideal conditions, where variations are only generated due to randomness in the process and systematic uncertainty due to measurement accuracy. Experimental set 2 is a set of multiple experiments, with each subset having a different value for a selected process parameter. For this work, the current is adjusted, which is one of the most influential process parameters of the process [8]. The rationale behind this case study is to prove the flexibility of the technique over a wide range of machine parameters. Experimental set 3 is a set of multiple experiments, with each subset having a geometrical adjustment of the electrode clamp, causing a variation in the static electrode bulk resistance (EBR), which is part of the secondary circuit. This is realised by adding custom build raisers (*shims*) between the electrode and its holder. Due to the principle of stacking multiple thin shims, the conductivity decreases significantly, causing the resistivity to increase with only a minor increase in extra material required. For the three examined cases, the resistance between two predetermined points, one above the added shims and one below the added shims, is measured to be 11.9, 108.4 and 371.5  $\mu\Omega$  respectively. This case is included to illustrate the

performance of the technique for a common problem in an industrial setting, where the change of welding electrodes or welding clamps inherently causes a variation in the overall resistance of the machine's electrical circuit. The welded specimen are low carbon steel samples of 20 by 70 mm and thickness of 1 mm and are welded in as-delivered condition. Data is acquired by a Dewetron DEWE2-a4L data acquisition system at a sampling rate of 2 MHz. Acquired signals include (1) electrical voltage over the welding electrodes and (2) electrical current in the welding circuit, measured by a PEM RFT 300S Rogowski coil and preamplifier.

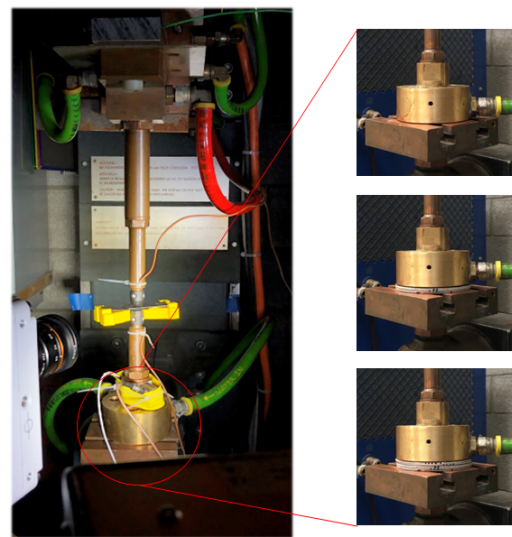


**Fig. 2:** Setup of the machine (left), with location of shims for experimental set 3 (right), top-down: zero, 3 and 5 shims.

All samples are labelled by physical measurements of the weld nugget diameters according to ISO 10447:2015 (*specifies the procedures and recommended tooling to be used for peel and chisel testing of resistance spot and projection welds. ISO 10447:2015 applies to welds made in two or more sheets in the thickness range of 0,5 mm to 3,0 mm*). The process parameters are chosen such that the nominal nugget diameters correspond to the welding lobe diagram according to ISO 14327:2004,  $3.5\sqrt{t}$ , with  $t$  the thickness of a single plate. Furthermore, the weld time and force differ greatly between the conducted experiments.

261 This is deliberately determined as such, to provide  
262 a demonstration on a case where the weld is gener-  
263 erated in a short time window as well as a case  
264 where a weld nugget is formed slower.

### 265 3 Dynamic resistance based 266 monitoring

267 This section describes, discusses and illustrates  
268 the geometrical attributes regression model as pre-  
269 sented in literature. It serves as a reference for the  
270 developments in the remainder of this work.

271 The geometrical attributes regression model  
272 is currently the most commonly adopted pre-  
273 diction model in industry. The model is based  
274 on input-output pairs, respectively from on-line  
275 measurements and nugget diameter measurements  
276 stemming from destructive testing (as elaborated  
277 in section 2). Figure 3 visualises the main flow of  
278 the approach. It consists of  $k$  welds being gener-  
279 ated and measured by means of an experimental  
280 campaign. The samples are *peeled*, a destructive  
281 testing method (ISO 10447:2015) for determin-  
282 ing the diameter of the weld nugget. When the  
283 demanded samples  $k$  are generated, the data is  
284 subjected to a training algorithm based on the  
285 input-output pairs. All additional samples ( $i \geq k$ )  
286 are then predicted based on the trained model.

#### 287 3.1 Feature extraction

Measurement of dynamic resistance is one of  
the most effective techniques for quality moni-  
toring and estimation, aided by the fact that  
measurements are straightforward, including elec-  
trical current and voltage in the secondary circuit.  
Next, the dynamic resistance signal is obtained  
according to Ohm's law, i.e.

$$R(t) = \frac{U(t)}{I(t)}, \quad (1)$$

288 with  $R(t)$  the dynamic resistance,  $U(t)$  the the  
289 voltage,  $I(t)$  the welding current and  $t$  the welding  
290 time.

291 During the process, the welding machine forms  
292 a closed circuit with the secondary circuit of a  
293 transformer, ensuring a solid mechanical assem-  
294 bly between tooling and work pieces. The closed  
295 circuit is modelled in terms of their individual

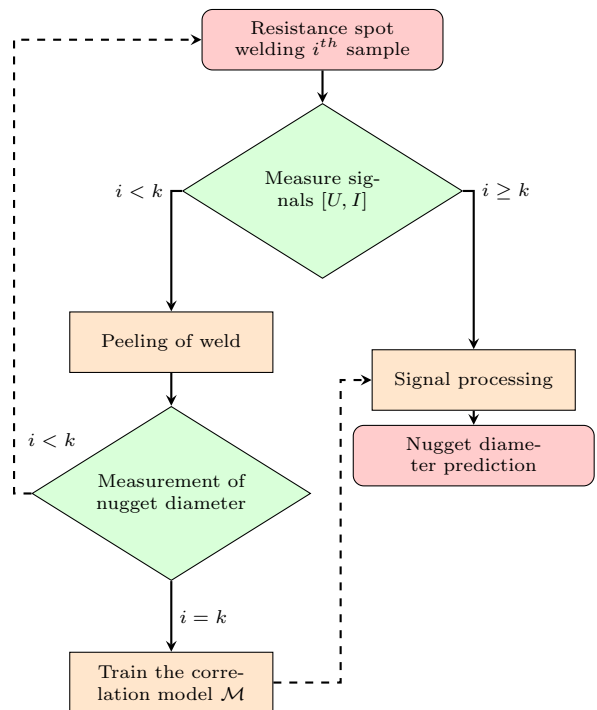
resistances. In this resistance model, the electri-  
cal resistances of the transformer, the mechanical  
assembly, and the work pieces are represented as  
respectively  $R_t$ ,  $R_m$  and  $R_l$ . The resistances  $R_t$   
and  $R_m$  are assumed constant during the process.  
The resistance of the work pieces is split into three  
components:

- 303 1. the bulk resistance of the sheet metal ( $R_b$ ),
- 304 2. the interface resistance between electrodes and  
305 sheet metal ( $R_c$ ),
- 306 3. the contact resistance of the parts surfaces  
307 ( $R_f$ ).

For the general case of two pieces of sheet  
metal, assumed equal in properties and dimen-  
sions, the resistance of the work pieces is:

$$R_l = 2R_b + 2R_c + R_f. \quad (2)$$

As illustrated in figure 1, there are multiple  
stages during the process, causing a large fluctua-  
tion of  $R_l$ . The geometrical attributes approach,

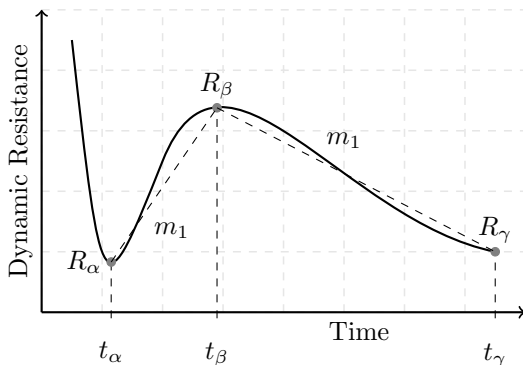


**Fig. 3:** Workflow a. General prediction model structure for RSW

**Table 1:** Overview of conducted experiments and their process parameters used in this paper. *EBR: Electrode bulk resistance setup, n: amount of welds*

No.	Current (kA)	Force (kN)	Time (ms)	EBR	N
1	7.2	5	210	cte	174
2	6.0 - 6.6 - 7.2	2.5	70	cte	50 - 50 - 50
3	7.6	2.5	80	var.	50 - 50 - 50

elaborated in section 3.2, refers to several points that characterise the dynamical resistance curve. Extracted points from the curve are based on e.g., peaks and slopes. Figure 4 illustrates several key points of the curve, respectively the initial peak  $R_0$  in phase 1, the pit  $R_\alpha$  in phase 2, the peak at the beginning of phase 4, also commonly known as the beta peak  $R_\beta$  and the last value of the DR curve  $R_\gamma$ , also respectively the times  $t_0$   $t_\alpha$ ,  $t_\beta$  and  $t_\gamma$ . Next, several critical derivatives are selected, the mean value  $R_m$ , the slopes  $m_1$  and  $m_2$  and the resistance variance  $dR1 = R_\beta - R_\alpha$  and  $dR2 = R_\gamma - R_\beta$

**Fig. 4:** Theoretical dynamic resistance curve, with selected features for the geometrical attributes approach, adopted from [9].

However, one drawback of this technique is that these measured parameters fluctuate heavily during a single weld due to the time-varying current generated by a mid frequency direct current (MFDC) power supply. The dynamic resistance, derived according to Eq. 1, is subjected to a signal filter in order to obtain the main trend. Zhang *et al.* [26] evaluated the raw signals and acknowledged, based on Fourier spectrum analysis, that periodic features are key to the large fluctuations. They applied a fourth-order digital low pass filter with a cut-off frequency of 50 Hz. For this

**Table 2:** Overview of correlations between derived features and the QI, based on experimental case 1

feature ( $f_i$ )	%	feature ( $f_i$ )	%
$t_0$	1.68	$R_0$	3.06
$t_\alpha$	-31.37	$R_\alpha$	33.36
$t_\beta$	-30.60	$R_\beta$	20.62
$t_\gamma$	-20.43	$R_\gamma$	-8.56
$m_1$	8.60	$m_2$	6.30
$dR1$	-4.45	$dR2$	49.73
$R_m$	44.29		

study, the concept of the moving average filtering is selected to eliminate the interference of periodic signals effectively [33].

### 3.2 Geometrical attributes model

Post-filtering the dynamic resistance signal provides a noise-free curve where the features described in section 3.1 (Figure 4) are observable. Table 2 gives an overview of the correlations between the features according to figure 4 and the QI, based on case 1 from table 1. This table shows that correlations between inputs and the QI are present. This confirms the applicability of the geometrical attributes approach, as discussed by [9]. The ensemble of these, or similarly derived, correlations, superseded with generic regression analysis, are current state of the art methods for RSW quality indication. This is visualised as the left part in figure 5. Part A, the feature selection, yields the aforementioned features of the dynamic resistance curve. Next, in part B, a multiple linear regression model describes the relationship between the features and the QI. The selection of features is case dependent, and relates to the most significant features of the curve, with a minimum of six points, without significantly affecting the model performance [9]. The regression model is described as

$$q = \beta_0 + \beta_1 f_1 + \beta_2 f_2 + \dots + \beta_k f_k + \varepsilon \quad (3)$$

with  $q$  the QI response,  $f$  the regressor variable,  $\beta$  the regression coefficients and  $\varepsilon$  the error term.

This overall workflow makes it possible to project new data-points onto the regression model and predict (interpolate) an estimate for the QI.

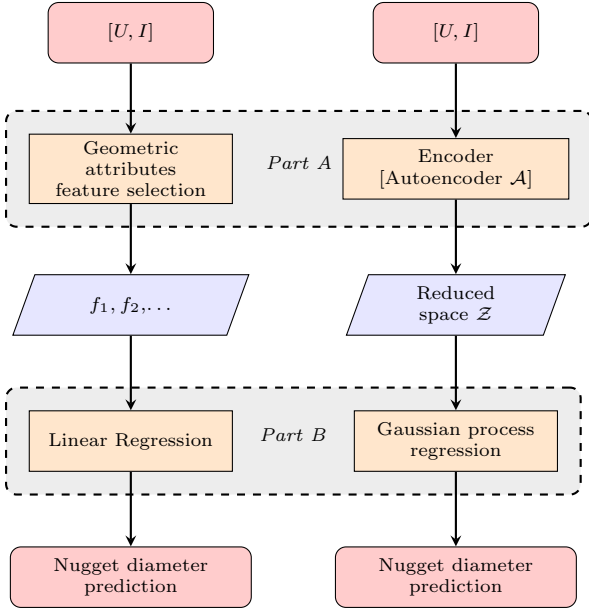


Fig. 5: Workflow b. Technical

## 4 Autoencoder based weld quality monitoring

This section discusses the main innovation of this study, replacing both part A and part B of the technique elaborated in section 3.2, as also illustrated in the right part of figure 5. In the following, the method is introduced and discussed, as well as illustrated based on experimental set 1 (table 1).

### 4.1 Part A: Feature extraction

#### 4.1.1 The curse of dimensionality

Part A in this work focuses on improving the amount of information that is extracted from the dynamic resistance curve. For this, an efficient coding is required that is capable of learning a low dimensional representation for a set of data. Opposed to the method of manually selecting

points, recent advances in deep learning methodologies are proven to be very efficient in gathering interesting features in the data, which are possibly unobservable or not detectable to the engineer during manual evaluation of the data. However, especially for this application, this poses specific challenges regarding the architecture of the network. Indeed, with a sampling rate of  $2Mhz$  and the process yielding  $> 200ms$  of welding time, a very high amount of data is gathered on multiple channels, which serves as the input of the network. The main problem is that the computational cost of the neural network scales exponentially with the data, by cause of a connection that is required to each neuron in the next layer, according to:

$$z_j^l = \varphi(v_j) = \varphi\left(\sum_{i=0}^k w_i \cdot z_i^{l-1}\right), \quad (4)$$

where  $z_j^l$  is the value  $z$  for neuron number  $j$  in layer  $l$ ,  $\varphi$  represents the activation function, usually a sigmoid function ranging from  $-1$  to  $1$ ,  $\varphi(v_j) = \frac{2}{(1+\exp(-2 \cdot v_j))} - 1$ ,  $z_i^{l-1}$  representing neuron number  $i$  from layer  $l-1$ ,  $w_i$  the weight assigned to each connection with the previous layer,  $k$  the number of neurons in layer  $l-1$  and  $z_0 = \pm 1$  for adding a bias  $b = w_0$  to the summation operator, yielding  $v_j$ . Evaluating this key equation is computationally not a large effort. However, due to the architecture of neural networks, it has to be solved numerous times during training. As such the total training effort is increased drastically. This is often referred to as the curse of dimensionality, referring to problems that occur when dealing with data in high-dimensional spaces. It prevents strategies to work efficiently, while creating problems concerning computational expenses, which do not occur in low-dimensional spaces.

Multiple techniques for dimensionality reduction exist. They can be divided into convex and non-convex techniques, where convex techniques optimise an objective function that does not contain any local optima, e.g., Principal Component Analysis (PCA), Kernel PCA, Isomaps, Local Linear Embedding (LLE) and non-convex techniques optimise objective functions that do contain local optima, e.g., Locally Linear Coordination (LLC), manifold charting or autoencoders [14, 28]. For a competent model, capable of being deployed in an on-line context, a marginal computation cost is

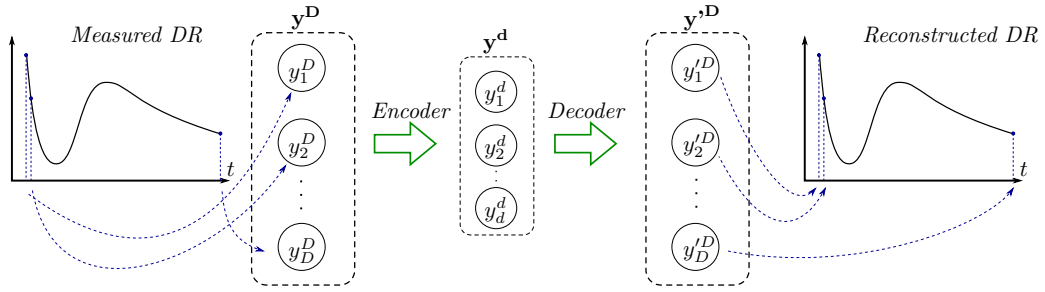


**Fig. 6:** Autoencoder topology

386 envisaged for the projection of a series of points 411  
 387 to the low dimensional space, but also the ability 412  
 388 to embed new high-dimensional data points into 413  
 389 an existing low-dimensional data representation is 414  
 390 important. For these reasons, autoencoders have 415  
 391 been selected for the dimension reduction in this 416  
 392 work.

#### 393 4.1.2 Autoencoder based dimension 419 394 reduction 420

395 Autoencoders, a type of artificial neural network, 421  
 396 are the proposed solution for this work, based 422  
 397 on their efficiency, non-linear transformation and 423  
 398 intuitive nature [2].

These feed-forward networks have an odd num-  
 ber of hidden layers  $hL_i$ , with  $i = 1 \dots n_l$  and  
 $n_l$  the amount of layers, where the hidden layers  
 are dimensioned such that the layer in the mid-  
 dle has a lower amount of neurons than the first  
 and last layer. This separates the autoencoder in  
 an input layer, an encoder part, the middle layer  
 with  $d \leq D$ , a decoder part and the reconstructed  
 layer:

$$\mathbf{y}^D \xrightarrow{\text{Encoder}} \mathbf{y}^d \xrightarrow{\text{Decoder}} \mathbf{y}'^D, \quad (5)$$

399 where  $\mathbf{y}^D$  is the measured data,  $D$  the number of 411  
 400 time-steps in the input data, and  $d$  the amount 412  
 401 of neurons in the middle layer. The objective of 413  
 402 the autoencoder is to generate this neural network 414  
 403 architecture such that  $\mathbf{y}'^D \approx \mathbf{y}^D$ . The autoen- 415  
 404 coder is an unsupervised learning technique, since 416  
 405 its goal is to minimise an error in reconstructing 417  
 406  $\mathbf{y}^D$ . The input layer  $\mathbf{y}^D$  has  $D$  neurons, where each 418  
 407 neuron represents an individual parameter from 419  
 408 the dataset. This data is reconstructed in the final 420  
 409 layer  $\mathbf{y}'^D$  of equal dimension  $D$ , as illustrated in 421  
 410 figure 6.

The centre layer in the network  $\mathbf{y}^d$  represents  
 the original data in a lower dimension  $d$ , while  
 preserving as much structure as possible from the  
 dataset  $\mathbf{y}^D$ . The resulting low dimensional repre-  
 sentation in this centre layer functions as the input  
 for further processing, which has the benefit of  
 working with far less data without losing essential  
 information.

Mapping from the input vector to another vec-  
 tor by means of an encoder, based on the general  
 equation of a neural network topology (eq 4) gives:

$$y^d = \varphi(W^1 y^D + b^1) \quad (6)$$

and for the reconstruction through a decoder:

$$y'^D = \varphi(W^2 y^d + b^2). \quad (7)$$

The network is trained by minimising a loss  
 function, which includes regularisation terms.  
 Apart from the mean squared error function, an  
 L2 regularisation term  $\lambda * \Omega_{weights}$  and sparsity  
 regularisation term  $\beta * \Omega_{sparsity}$  are added to the  
 loss function. The L2 regularisation term forces  
 the weights to remain small, by adding a penalty  
 to the loss function when weights are increas-  
 ing. The sparsity regularisation term attempts to  
 enforce a constraint on the sparsity of the out-  
 put from the hidden layer. The cost function for  
 training the autoencoder based on  $N$  samples  
 yields

$$\begin{aligned} \mathcal{L}(y^D, y'^D) = & \frac{1}{N} \sum_{n=1}^N \sum_{j=1}^D (y_{jn}^D - y'_{jn})^2 \\ & + \lambda * \Omega_{weights} + \beta * \Omega_{sparsity} \end{aligned} \quad (8)$$

with  $\lambda$  the coefficient for the L2 regularization term and  $\beta$  the coefficient for the sparsity regularization term.

The workflow for applying this metric for the dynamic resistance curve is illustrated in figure 7.

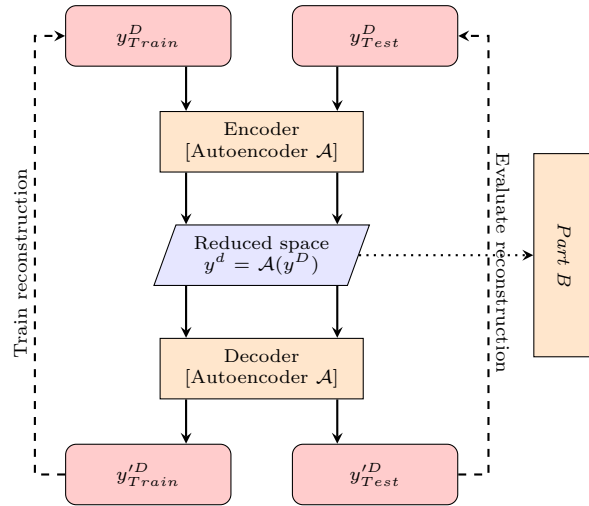


**Fig. 7:** Workflow c. Autoencoder training principle

In this figure, there is a clear distinction between the data for training and testing. It also indicates the main workflow, where eq. 8 is used to train the reconstruction of the measured signal and to evaluate the reconstruction of test data. Furthermore, the figure illustrates that part B is connected to the low dimensional layer, in the centre of the autoencoder.

### 4.1.3 Illustration

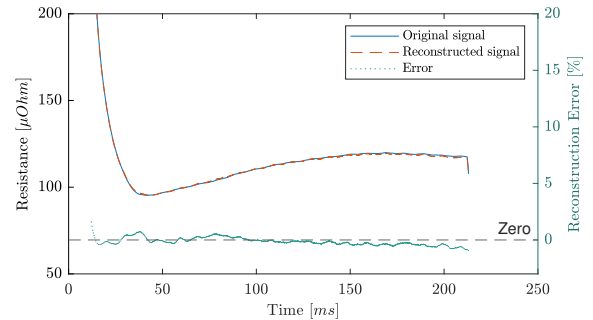
The autoencoder based dimension reduction is now illustrated based on experimental case 1 from table 1. Out of 174 experiments, 90 % serves as training data, whereas the remaining 10 % is test-data to evaluate the performance.

Figure 8 illustrates the performance of the network for one sample from  $y_{Test}^D$ , where one dynamic resistance curve is plotted next to its reconstructed counterpart. Since the error is nearly negligible, the instantaneous reconstruction

error  $\epsilon_{AE}$  is given, defined as:

$$\epsilon_{AE} = \frac{y'^D - y^D}{y^D} \cdot 100. \quad (9)$$

In this example, the signal is compressed from  $D = 450.000$  data-points into a middle layer of the autoencoder, represented by  $y^d$ , where  $d = 15$ . The hyper-parameters for the network are summarised in table 3.



**Fig. 8:** Measured and reconstructed signal with means of an autoencoder network, with topology  $450k - 15 - 450k$

Note that the reconstruction is only required for training of the autoencoder. For the purpose of dimensionality reduction, the encoder projection, resulting in the reduced space  $y^d$  is an important step to come to an efficient regression model, as illustrated in figure 7.

At this point, it can be concluded that the presented method is capable of projecting the measured dataset into a reduced space  $y^d$ , which acts as a low dimensional space. The reconstructed projected data, by means of the autoencoder, performs approximately equal to the measured data, as the error is nearly negligible. Furthermore, the projected data contains nearly all information to reconstruct the data in a low dimensional space, thus possessing at least as valuable information as the manually determined points, as described in section 3.2. Therefore, the reduced space  $y^d$  can serve as an input to current the QI prediction step using generalised techniques, e.g., multiple regression. It should be noted that the projected data has no physical meaning in the process, opposed to the selected features from section 3.2. The added benefit of this method is the robustness of

**Table 3:** Hyperparameters for training Autoencoder

Encoder-TF	<i>Sigmoid</i>
Decoder-TF	<i>Sigmoid</i>
$d$	15
L2 weight coef. $[\lambda]$	0.009
Sparsity Proportion $[\hat{\rho}_i]$	0.719
Sparsity Regularization $[\beta]$	1.08
Normalised data	<i>Yes</i>

the algorithm, which is unlikely to suffer abnormalities, e.g. where expulsion could cause an effect in the curve, resulting in misjudgement or wrong interpretation of the data. Additionally, the measured signal is prone to various effects like time shift, originated during the processing of the data, caused by the required filtering techniques of the signal. The presented approach is also insensitive to these effects.

## 4.2 Part B: QI prediction

Part B of the novel prediction model (see figure 5) requires an algorithm capable of giving a robust regression between input-output, respectively the measured signals during the welding process projected on a reduced space  $\mathcal{Z}$  by means of an autoencoder, and the measured nugget diameter of the weld (QI). Due to the low amount of available labelled data, training a neural network based on input-output pairs tends to be troublesome, in particular overfitting is a main concern. This should not be confused with the neural network on which the autoencoder from section 4.1 is based, as the latter is an unsupervised technique, which does not require labelled data.

### 4.2.1 Gaussian Process Regression

A powerful tool, ideal for this problem is Gaussian Process Regression (GPR). In its original form, Gaussian Process modelling is a statistical interpolation method that exploits Gaussian processes to interpolate a series of complex functions. The technique works well on small datasets, and has the capability to provide uncertainty metrics on the predictions. Gaussian process modelling, also known as Kriging, was introduced in the context of meta-modelling in the works of Sacks et al. [19], in which the original form of Kriging, as developed in the Master's thesis of D. Krige [16], served as a backbone to represent an input/output mapping

of an expensive computational model. For application in machine learning, Kriging has evolved as both regression and classification tool, and has proven to be a treasured algorithm [18].

The required dataset  $\mathcal{D}$  with  $N$  observation is presented as

$$\mathcal{D} = \{(y_i^d, q_i) | i = 1, \dots, N\} \quad (10)$$

with  $y_i^d$  the vector with multiple input variables and  $q_i$  as a measure for the QI, which is continuous, as this is a regression case.

In essence, GPR serves as an interpolation model for a regression problem mapping the QI on the variables.

Their key equation of GPR is presented as:

$$q = \mathcal{M}(y) + \varepsilon, \quad (11)$$

with  $\mathcal{M}(x)$  the GP model. It is assumed that the observed responses are noisy and the noise  $\varepsilon$  follows a zero-mean Gaussian distribution

$$\varepsilon \sim \mathcal{N}(0, \sum_n), \quad (12)$$

where  $\sum_n$  is the covariance matrix of the noise term. For this work, the noise variance is identified as general heteroscedastic, in which the noise can differ for each observed response. For a more in depth study of GPR, the reader is referred to the citations in previous section.

An important feature of this type of model is the applicability of K-fold cross-validation. The main idea of this is to re-evaluate the model with a subset of the training data. This allows to optimise the hyper-parameters of the model, based on evaluating the model with each subset of data, thus minimising a cross-validation error. This yields a model, capable of working under limited data, and providing efficient predictors with minimal effort, unlikely to suffer from overfitting. Performance-wise, training this model takes significantly longer than linear regression. However, as elaborated in the introduction, the computational requirement for training is irrelevant for an in-line paradigm. What is of interest is the required time to evaluate a single sample. This will be studied for the illustrative data set in the next section.

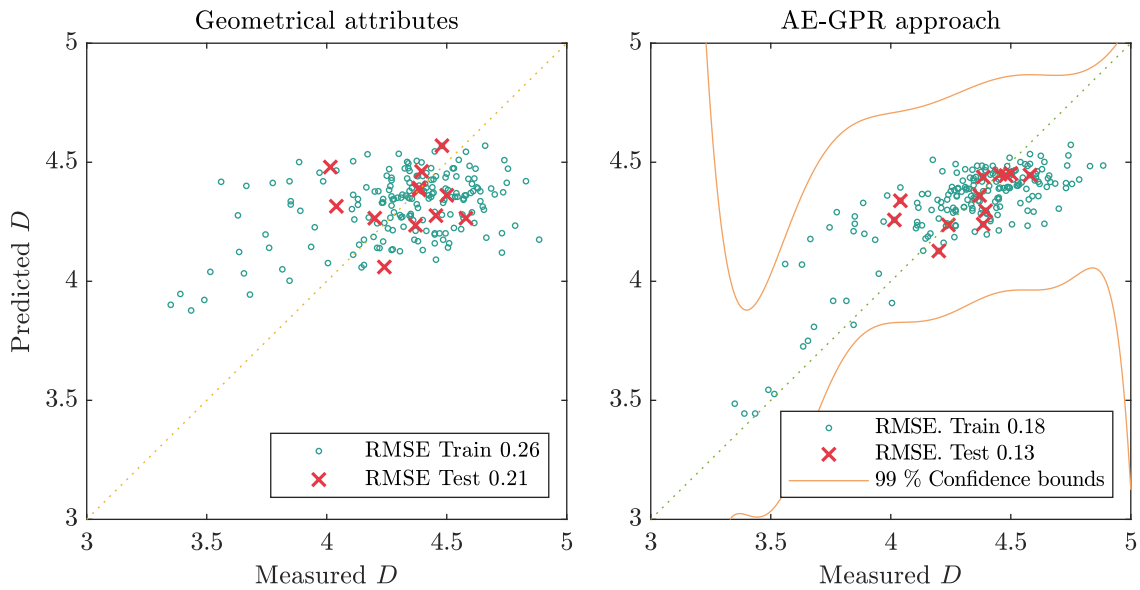


**Fig. 9:** Predicted vs. actual QI based on the AE-GPR approach (*right*) compared to the Geometrical attributes approach (*left*) for the reference case

#### 4.2.2 Illustration

The methodology is presented on the data resulting from section 4.1.3. Computation experiments and the training of the proposed algorithms are performed on a server, consisting of 2 AMD Epyc 7601 32-core CPU's, 512 GB memory and an NVIDIA Tesla V100 - 32 GB graphical accelerator. For benchmarking computational effort of the proposed algorithm, the system is limited to only 1 core, while GPU acceleration is disabled.

The summary of computational costs for both the reference and the newly developed approach are given in table 4. Comparison of the required time for the regression approaches clearly reveals that the GPR technique is more expensive. This is due to the fact that substantially more time is required to determine the optimal hyperparameters, compared to the key, and only equation required for multiple linear regression 3. Apart from that, the table also shows that especially the training of the unsupervised deep learning based dimension reduction technique into an autoencoder (AE) necessitates a high performance computational device. However, the cost for training is only a small investment for a continuously guarded process. Table 4 also summarises the computational costs for training and propagating a single

**Table 4:** Computational costs for the framework, *AE*: Autoencoder based dimension reduction, *GPR*: Gaussian Process Regression

		Training	1 Sample
<i>Part A</i>	Geom. attributes	$1.8 \times 10^3$ s	0.46 s
	AE	$5 \times 10^4$ s	0.83 s
<i>Part B</i>	Linear regression	1.01 s	0.03 s
	GPR	91 s	0.04 s

sample. This shows that propagating a single experiment through the full AE-GPR framework requires only a marginally higher cost compared to the approach based on the geometrical attributes.

In order to assess the performance of the developed method, figure 9 illustrates the correlation between the predicted QI and the measured QI, both for the geometrical attributes approach (*left*) and the novel AE-GPR approach (*right*).

A clear improvement over the geometrical approach is noticeable. Not only does the Root Mean Squared Error (RMSE) improve vastly, from 0.26 to 0.18, it is also clearly visible that the geometrical approach fails to predict the overall nugget diameter. Specifically, the graph based on the geometrical approach shows a horizontal scatter, indicating a larger spread on the measured QI, but a small spread on the predicted

586 QI. Furthermore, in addition to the continuous 633  
 587 mean regressor estimate by the GPR model, also 634  
 588 confidence bounds are provided, based on the 635  
 589 available training data and known variance of the 636  
 590 GPR model. For this case, the 99 % bounds are 637  
 591 provided, showing a narrow band encapsulating 638  
 592 the data. As a final verification, the algorithm 639  
 593 is subjected to several testing points, which were 640  
 594 excluded from the training. The latter is rep- 641  
 595 resented by 10 % of the available data and is 642  
 596 visualised by the red crosses. The RMSE for the 643  
 597 test points improves from 0.21 to 0.13 for the test 644  
 598 data, which emphasises the performance of the 645  
 599 model by resulting in a prediction well within the 646  
 600 bounds predicted by the algorithm. 647

## 601 5 Verification of the proposed 649 602 method 650

603 To benchmark the accuracy and robustness of the 652  
 604 introduced approach, the algorithm is subjected to 653  
 605 two more cases. Compared to case 1 of section 3.2 654  
 606 for which an experimental set with fixed process 655  
 607 parameters was used (thus only yielding process 656  
 608 variability on both input and output), the next 657  
 609 two cases include highly relevant industrial events 658  
 610 representing common process variations.

### 611 5.1 Current variation 659

612 This case (table 1, No.2) is a dataset combin- 660  
 613 ing data from three consecutive experimental runs 661  
 614 with respectively altering the current as described 662  
 615 in table 1. The goal of this case is to determine 663  
 616 the robustness of the AE-GPR approach based on 664  
 617 a broader set of input signals, as could be the 665  
 618 case in an industrial setup where low- and flexible 666  
 619 production is key and in-line monitoring is envis- 667  
 620 aged. First, applying a dimension reduction on the 668  
 621 measured signals reduces the dataset from 450.000 669  
 622 samples to 15, while only losing  $< 1$  % of infor- 670  
 623 mation, based on mean-squared error estimates. 671  
 624 This is illustrated in figure 11, where the origi- 672  
 625 nal curve, the reconstructed curve and the error 673  
 626 are illustrated. Analysing the measured and pre- 674  
 627 dicted data, illustrated in figure 10, clearly reveals 675  
 628 several meaningful results. 676

629 First, no separate data clusters can be dis- 677  
 630 tinguished according to the difference in welding 678  
 631 currents. Yet, the three datasets are separated 679  
 632 by colour, which reveals the difference in nugget

diameter in function of process parameters. Sec-  
 ond, the measured results with  $6.0kA$  and  $7.2kA$   
 have a wider spread of data compared to the  
 set welded with  $6.6kA$ . Third, advancing to the  
 results of the prediction model, there is a clear  
 improvement of the AE-GPR method over the  
 geometrical approach. The RMSE is improved ,  
 from 0.39 to 0.13. It is clearly visible that the  
 predictions based on the AE-GPR approach are  
 more confined than the predictions based on the  
 geometrical approach. Furthermore, the predictor  
 based on the geometrical approach fails clearly in  
 determining the measured nugget diameter on the  
 samples stemming from the subset yielding the  
 smallest nugget diameter. The provided 99 % con-  
 fidence bounds show a narrow band encapsulating  
 the data.

As a final verification, the algorithm is sub-  
 jected to several testing points which were  
 excluded from the training. The latter is rep-  
 resented by 10 % of the available data and is  
 visualised by the red crosses. The RMSE for the  
 test points improves from 0.62 to 0.13 for testing  
 data. Both the RMSE and graphical representa-  
 tion of the predicted value indicate a prediction  
 well within the predicted bounds of the algorithm.

### 659 5.2 EBR variation 660

For the final example, a highly relevant industrial  
 case is elected. One of the advantages of many  
 state-of-the-art welding controllers is their ability  
 to monitor themselves and intervene during a single  
 weld. This is required to achieve a certain thresh-  
 old of total current flow and is often realised by  
 extending the weld time or increasing the current.  
 An important reason why this threshold is often  
 not achieved is the variation in the closed loop  
 resistance in the secondary circuit. These varia-  
 tions affect the welding process and potentially the  
 reaction of the controller, causing a variation in  
 the weld nugget diameter. Also, it is well known  
 within RSW industry that the weld nugget diame-  
 ter is negatively affected by variation in the closed  
 loop resistance in the secondary circuit. The latter  
 is often a consequence of machine disturbances,  
 e.g., maintenance, re-torquing or swapping tools.  
 Thus re-calibration is required when adjustments  
 are made to the welding heads to counter this

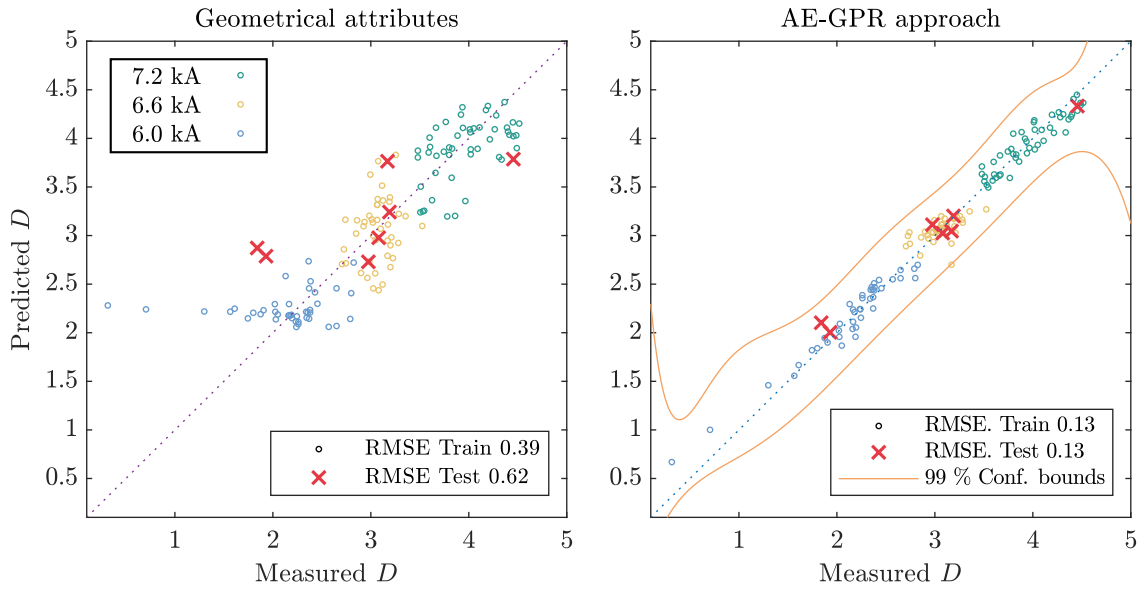


**Fig. 10:** Predicted vs. actual QI based on the AE-GPR approach (*right*) compared to the Geometrical attributes approach (*left*) for the current variation case

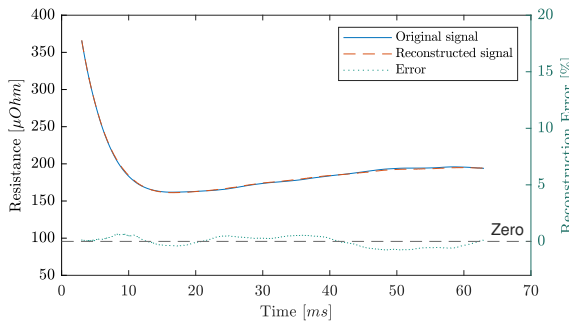


**Fig. 11:** Measured and reconstructed signal with means of an autoencoder network, with topology  $450k - 15 - 450k$  for the current variation case

in figure ???. This variation is a constant resistance during the process and is part of  $R_m$ , as elaborated in section 3.1.

Analysing the measured and predicted data, illustrated in figure 12, clearly reveals several meaningful results. First, the influence of the change from  $11.9$  to  $108.4\mu\Omega$  has an almost negligible effect on the measured nugget diameter with respectively an average of  $4.24$  and  $4.09\text{ mm}$  and equal standard deviation of  $0.18\text{ mm}$ . The experiments where the resistance is increased to  $371.5\mu\Omega$  indicate a noticeably smaller nugget diameter, with an average of  $3.18\text{ mm}$  and standard deviation of  $0.33\text{ mm}$ . Second, applying the proposed dimension reduction by means of a trained autoencoder reduces the dataset from  $140.000$  samples to  $30$ , while only losing  $< 1\%$  of information, based on mean-squared error estimates.

Third, advancing to the results of the prediction model, there is a clear improvement over the geometrical approach. For the set with  $11.9$  and  $108.4\mu\Omega$ , the variation in nugget diameter is rather low, yet the AE-GPR is capable of predicting the nugget diameter more accurate compared to the geometrical approach. The nugget diameters for the set with  $371.5\mu\Omega$  range from  $2.7$

680 effect. The goal of this third case is to demon-  
681 strate the potential of our approach when the  
682 aforementioned effects are present.

683 The dataset is a combination of three consec-  
684 utive experimental runs altering the resistance of  
685 the secondary circuit by means of custom shims  
686 between the welding head and electrode holder,  
687 while the compensation of the controller is dis-  
688 abled. The resistance between two fixed points in  
689 the mechanical assembly is respectively measured  
690 to be  $11.9$ ,  $108.4$  and  $371.5\mu\Omega$ . This is achieved  
691 by respectively zero, 3 and 5 shims, as illustrated

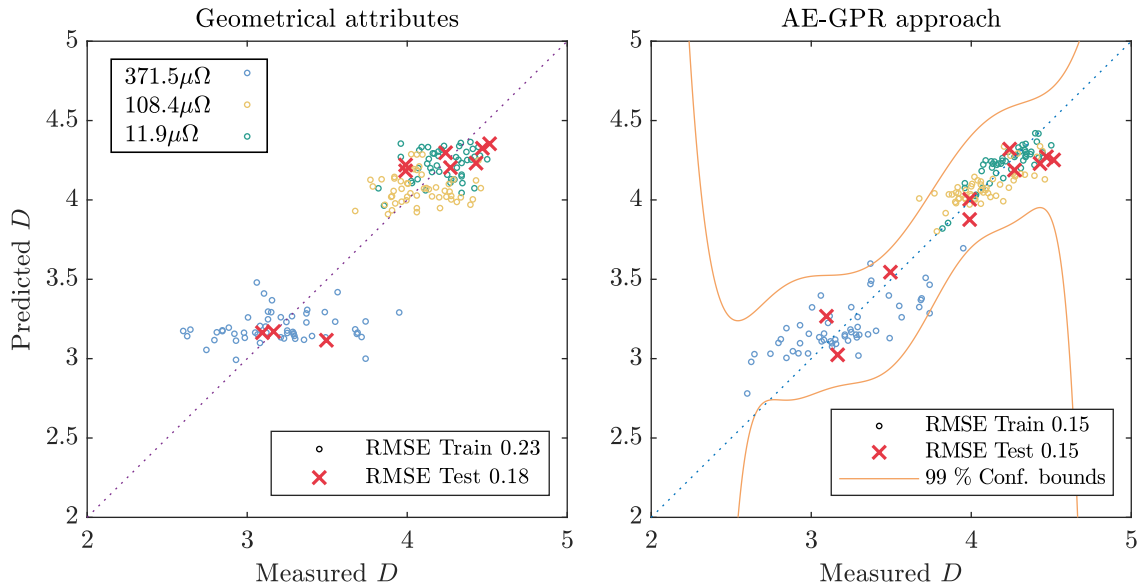


**Fig. 12:** Predicted vs. actual QI based on the AE-GPR approach (*right*) compared to the Geometrical attributes approach (*left*) for the EBR variation case

718 to 4.1 mm, while the geometrical approach pre- 743  
 719 dicted only between 3.0 and 3.5 mm. The AE-GPR 744  
 720 approach predicts this set, both for the training 745  
 721 and test points. The RMSE of the predictions 746  
 722 improves clearly, from 0.23 to 0.15. For this case, 747  
 723 the 99% bounds are provided, showing a narrow 748  
 724 band encapsulating the data. 749

725 The test points are represented by 10 % of 750  
 726 the available data. The RMSE for the test points 751  
 727 improves from 0.18 to 0.15, resulting in a pre- 752  
 728 diction well within the predicted bounds of the 753  
 729 algorithm. 754

## 730 6 Conclusion

731 This paper presents a novel approach for an effec- 758  
 732 tive predictor for the nugget diameter, i.e., the 759  
 733 main quality indicator (QI) of a resistance spot 760  
 734 welding process, based on on-line measured pro- 761  
 735 cess data. The most important feature of the 762  
 736 developed methodology is the combination of 763  
 737 deep learning for dimension reduction, and the 764  
 738 consequent machine learning prediction tool. We 765  
 739 demonstrate how to use unsupervised deep learn- 766  
 740 ing in the form of an autoencoder to discover 767  
 741 a low-dimensional transformation in which the 768  
 742 parameters characterise a pattern that embodies

underlying information on the process, possibly 743  
 unobservable or not detectable by any other cur- 744  
 rently existing approach. The underlying informa- 745  
 tion is transformed into a low dimensional space, 746  
 which is an ideal scene for a Gaussian process 747  
 regression model linking the input data through 748  
 the autoencoder to the measured nugget diam- 749  
 eter. The model is trained on a limited set of 750  
 data, leading to a low cost implementation in 751  
 an industrial setting. The technique is presented 752  
 in an example case which clearly indicates that 753  
 it leads to an improved QI prediction compared 754  
 to the state of the art geometrical attributes 755  
 approach. The technique is presented on two addi- 756  
 tional cases, each pinpointing a specific bottleneck 757  
 within industry related to the RSW process. Both 758  
 cases are analysed and indicate very promising 759  
 results, where the new AE-GPR approach has 760  
 consistently improved results over the geometrical 761  
 approach. It should be noted that the time to train 762  
 the proposed model is substantially higher. How- 763  
 ever, the investment cost is rather low compared 764  
 to the benefit in an in-line monitoring system. 765  
 We conclude that the proposed method can be 766  
 readily applied to an in-line context for quality 767  
 assessment in industrial RSW applications, as the 768

769 time for evaluating in an in-line context is suit- 811  
 770 able, and accuracy is vastly improved over existing 812  
 771 techniques. 813

## 772 7 Acknowledgements 814

773 This work was funded by KU Leuven, grant 815  
 774 #C24E/21/026. 816

775 **Conflict of interest:** The authors declare no 818  
 776 conflict of interest. 819

## 777 References 820

778 [1] Almeida FA, De Paula TI, Leite RR, et al 822  
 779 (2018) A multivariate GR&R approach to 823  
 780 variability evaluation of measuring instru- 824  
 781 ments in resistance spot welding pro- 825  
 782 cess. *Journal of Manufacturing Processes* 826  
 783 36(November):465–479. [https://doi.org/10.](https://doi.org/10.1016/j.jmapro.2018.10.030)  
 784 [1016/j.jmapro.2018.10.030](https://doi.org/10.1016/j.jmapro.2018.10.030), URL [https://doi.](https://doi.org/10.1016/j.jmapro.2018.10.030)  
 785 [org/10.1016/j.jmapro.2018.10.030](https://doi.org/10.1016/j.jmapro.2018.10.030) 827

786 [2] Bogaerts L, Faes M, Moens D (2019) A fast 830  
 787 inverse approach for the quantification of set- 831  
 788 theoretical uncertainty. In: 2019 IEEE Sym- 832  
 789 posium Series on Computational Intelligence 833  
 790 (SSCI), IEEE, pp 768–775 834

791 [3] Brunton SL, Kutz JN (2019) Data-driven 835  
 792 science and engineering: Machine learning, 836  
 793 dynamical systems, and control. Cambridge 837  
 794 University Press 838

795 [4] Chen S, Sun T, Jiang X, et al (2016) Online 839  
 796 monitoring and evaluation of the weld qual- 840  
 797 ity of resistance spot welded titanium alloy. 841  
 798 *Journal of Manufacturing Processes* 23:183– 842  
 799 191. [https://doi.org/10.1016/j.jmapro.2016.](https://doi.org/10.1016/j.jmapro.2016.06.003)  
 800 [06.003](https://doi.org/10.1016/j.jmapro.2016.06.003) 843

801 [5] Cho Y, Rhee S (2002) Primary circuit 845  
 802 dynamic resistance monitoring and its appli- 846  
 803 cation to quality estimation during resistance 847  
 804 spot welding. *Welding Journal (Miami, Fla)* 848  
 805 81(6)

806 [6] Cho Y, Rhee S (2004) Quality estimation 850  
 807 of resistance spot welding by using pat- 851  
 808 tern recognition with neural networks. *IEEE*  
 809 *Transactions on Instrumentation and Mea-*  
 810 *surement* 53(2):330–334

[7] Dejans A, Kurtov O, Van Rymenant P  
 (2021) Acoustic emission as a tool for pre-  
 diction of nugget diameter in resistance spot  
 welding. *Journal of Manufacturing Processes*  
 62(September 2020):7–17. [https://doi.org/](https://doi.org/10.1016/j.jmapro.2020.12.002)  
[10.1016/j.jmapro.2020.12.002](https://doi.org/10.1016/j.jmapro.2020.12.002), URL [https://](https://doi.org/10.1016/j.jmapro.2020.12.002)  
[doi.org/10.1016/j.jmapro.2020.12.002](https://doi.org/10.1016/j.jmapro.2020.12.002)

[8] Dickinson DW, Franklin JE, Stanya A (1980)  
 Characterization of Spot Welding Behavior  
 By Dynamic Electrical Parameter Monitor-  
 ing. *Welding Journal (Miami, Fla)* 59(6)

[9] El Ouafi A, Belanger R, Guillot M (2012)  
 Dynamic resistance based model for on-line  
 resistance spot welding quality assessment.  
*Materials Science Forum* 706-709:2925–2930.  
[https://doi.org/10.4028/www.scientific.net/](https://doi.org/10.4028/www.scientific.net/MSF.706-709.2925)  
[MSF.706-709.2925](https://doi.org/10.4028/www.scientific.net/MSF.706-709.2925)

[10] Ghaffari B, Mozurkewich G (2010) Non-  
 destructive evaluation of spot-weld quality.  
 In: *Failure mechanisms of advanced welding*  
 processes. Elsevier, p 101–136

[11] Gomes GF, Viéville P, Durrenberger L (2017)  
 Dynamic behavior investigation of spot weld-  
 ing machines and its influence on weld cur-  
 rent range by modal analysis. *Journal of the*  
*Brazilian Society of Mechanical Sciences and*  
*Engineering* 39(3):765–773. [https://doi.org/](https://doi.org/10.1007/s40430-016-0580-0)  
[10.1007/s40430-016-0580-0](https://doi.org/10.1007/s40430-016-0580-0)

[12] Hamedi M, Atashparva M (2017) A review  
 of electrical contact resistance modeling  
 in resistance spot welding. *Welding in*  
*the World* 61(2):269–290. [https://doi.org/10.](https://doi.org/10.1007/s40194-016-0419-4)  
[1007/s40194-016-0419-4](https://doi.org/10.1007/s40194-016-0419-4), URL [http://dx.doi.](http://dx.doi.org/10.1007/s40194-016-0419-4)  
[org/10.1007/s40194-016-0419-4](http://dx.doi.org/10.1007/s40194-016-0419-4)

[13] Hao M, Osman KA, Boomer DR, et al (1996)  
 Developments in characterization of resis-  
 tance spot welding of aluminum. *Welding*  
*Journal (Miami, Fla)* 75(1):1–s

[14] Hinton GE, Salakhutdinov RR (2006) Reduc-  
 ing the dimensionality of data with neural  
 networks. *science* 313(5786):504–507

- 852 [15] Ighodaro OLR, Biro E, Zhou YN (2017) 896  
853 Study and Applications of Dynamic Resis- 897  
854 tance Profiles During Resistance Spot Weld- 898  
855 ing of Coated Hot-Stamping Steels. Met- 899  
856 allurgical and Materials Transactions A: 900  
857 Physical Metallurgy and Materials Sci- 901  
858 ence 48(2):745–758. [https://doi.org/10.1007/](https://doi.org/10.1007/s11661-016-3899-3)  
859 [s11661-016-3899-3](https://doi.org/10.1007/s11661-016-3899-3)
- 860 [16] Krige DG (1951) A statistical approach 904  
861 to some basic mine valuation problems on 905  
862 the witwatersrand. Journal of the Southern 906  
863 African Institute of Mining and Metallurgy 907  
864 52(6):119–139
- 865 [17] Ling SF, Wan LX, Wong YR, et al (2010) 908  
866 Input electrical impedance as quality mon- 909  
867 itoring signature for characterizing resis- 910  
868 tance spot welding. Ndt & E International 911  
869 43(3):200–205 912  
913  
914
- 870 [18] Rasmussen CE, Williams CK (2006) Gaus- 915  
871 sian Processes for Machine Learning, vol 1. 916  
872 MIT press 917
- 873 [19] Sacks J, Welch WJ, Mitchell TJ, et al (1989) 918  
874 Design and analysis of computer experiments. 919  
875 Statistical science 4(4):409–423 920
- 876 [20] Saxe AM, Bansal Y, Dapello J, et al (2019) 921  
877 On the information bottleneck theory of deep 922  
878 learning. Journal of Statistical Mechanics: 923  
879 Theory and Experiment 2019(12):124,020 924
- 880 [21] Wan X, Wang Y, Zhao D, et al (2017) Weld 925  
881 quality monitoring research in small scale 926  
882 resistance spot welding by dynamic resistance 927  
883 and neural network. Measurement: Journal 928  
884 of the International Measurement Confed- 929  
885 eration 99:120–127. [https://doi.org/10.1016/](https://doi.org/10.1016/j.measurement.2016.12.010)  
886 [j.measurement.2016.12.010](https://doi.org/10.1016/j.measurement.2016.12.010), URL [http://dx.](http://dx.doi.org/10.1016/j.measurement.2016.12.010)  
887 [doi.org/10.1016/j.measurement.2016.12.010](http://dx.doi.org/10.1016/j.measurement.2016.12.010) 930  
931  
932
- 888 [22] Wang SC, Wei PS (2001) Modeling dynamic 933  
889 electrical resistance during resistance spot 934  
890 welding. Journal of Heat Transfer 123(3):576– 935  
891 585. <https://doi.org/10.1115/1.1370502> 936
- 892 [23] Xia YJ, Su ZW, Li YB, et al (2019) Online 937  
893 quantitative evaluation of expulsion in 938  
894 resistance spot welding. Journal of Manu- 939  
895 facturing Processes 46(August):34–43. <https://doi.org/10.1016/j.jmapro.2019.08.004>,  
URL <https://doi.org/10.1016/j.jmapro.2019.08.004>
- [24] Xia YJ, Zhou L, Shen Y, et al (2021) 900  
Online measurement of weld penetration in 901  
robotic resistance spot welding using elec- 902  
trode displacement signals. Measurement: 903  
Journal of the International Measurement 904  
Confederation 168(September 2020):108,397. 905  
[https://doi.org/10.1016/j.measurement.](https://doi.org/10.1016/j.measurement.2020.108397)  
2020.108397, URL [https://doi.org/10.1016/](https://doi.org/10.1016/j.measurement.2020.108397)  
[j.measurement.2020.108397](https://doi.org/10.1016/j.measurement.2020.108397)
- [25] Xing B, Xiao Y, Qin QH, et al (2018) 908  
Quality assessment of resistance spot weld- 909  
ing process based on dynamic resistance sig- 910  
nal and random forest based. International 911  
Journal of Advanced Manufacturing Techno- 912  
logy 94(1-4):327–339. [https://doi.org/10.](https://doi.org/10.1007/s00170-017-0889-6)  
[1007/s00170-017-0889-6](https://doi.org/10.1007/s00170-017-0889-6)
- [26] Zhang H, Hou Y, Yang T, et al (2018) 915  
Welding quality evaluation of resistance spot 916  
welding using the time-varying inductive 917  
reactance signal. Measurement Science and 918  
Technology 29(5). [https://doi.org/10.1088/](https://doi.org/10.1088/1361-6501/aaa830)  
[1361-6501/aaa830](https://doi.org/10.1088/1361-6501/aaa830)
- [27] Zhao D, Wang Y, Lin Z, et al (2013) An 921  
effective quality assessment method for small 922  
scale resistance spot welding based on process 923  
parameters. Ndt & E International 55:36–41 924
- [28] Zhao D, Bezgans Y, Wang Y, et al (2020) 925  
Performances of dimension reduction tech- 926  
niques for welding quality prediction based 927  
on the dynamic resistance signal. Journal of 928  
Manufacturing Processes 58:335–343 929
- [29] Zhao D, Bezgans Y, Wang Y, et al 930  
(2021) Research on the correlation between 931  
dynamic resistance and quality estimation 932  
of resistance spot welding. Measurement 933  
168:108,299 934
- [30] Zhou K, Cai L (2013) Online nugget diame- 935  
ter control system for resistance spot welding. 936  
International Journal of Advanced Manufac- 937  
turing Technology 68(9-12):2571–2588. <https://doi.org/10.1007/s00170-013-4886-0>

- 940 [31] Zhou K, Cai L (2014) Study on effect of elec-  
941 trode force on resistance spot welding pro-  
942 cess. *Journal of Applied Physics* 116(8):1–7.  
943 <https://doi.org/10.1063/1.4893968>
- 944 [32] Zhou K, Yao P (2019) Overview of recent  
945 advances of process analysis and qual-  
946 ity control in resistance spot welding.  
947 *Mechanical Systems and Signal Process-*  
948 *ing* 124:170–198. [https://doi.org/10.1016/j.](https://doi.org/10.1016/j.ymsp.2019.01.041)  
949 [ymssp.2019.01.041](https://doi.org/10.1016/j.ymsp.2019.01.041), URL [https://doi.org/10.](https://doi.org/10.1016/j.ymsp.2019.01.041)  
950 [1016/j.ymsp.2019.01.041](https://doi.org/10.1016/j.ymsp.2019.01.041)
- 951 [33] Zhou L, Zheng W, Li T, et al (2020) A  
952 material stack-up combination identification  
953 method for resistance spot welding based  
954 on dynamic resistance. *Journal of Manufac-*  
955 *turing Processes* 56(March):796–805. [https:](https://doi.org/10.1016/j.jmapro.2020.04.051)  
956 [//doi.org/10.1016/j.jmapro.2020.04.051](https://doi.org/10.1016/j.jmapro.2020.04.051),  
957 URL [https://doi.org/10.1016/j.jmapro.2020.](https://doi.org/10.1016/j.jmapro.2020.04.051)  
958 [04.051](https://doi.org/10.1016/j.jmapro.2020.04.051)